LIMNOLOGY and OCEANOGRAPHY

ASLO

Limnol. Oceanogr. 9999, 2019, 1–9

doi: 10.1002/lno.11153

Size dependence of metabolism within marine picoplankton populations

John R. Casey,* Karin M. Björkman, Sara Ferrón, David M. Karl

Daniel K. Inouye Center for Microbial Oceanography, University of Hawai'i, Manōa, Honolulu, Hawaii

Abstract

Cell size is broadly applied as a convenient parameterization of ecosystem models and is widely applicable to constrain the activities of organisms spanning large size ranges. However, the size structure of the majority of the marine picoplankton assemblage is narrow and beneath the lower size limit of the empirical allometric relationships established so far (typically >1 μm). We applied a fine-resolution (0.05 μm increments) size fractionation method to estimate the size dependence of metabolic activities of picoplankton populations in the 0.10–1.00 μm size interval within the surface North Pacific Subtropical Gyre microbial assemblage. Group-specific carbon retained on each filter was quantified by flow cytometric conversion of light scatter to cellular carbon quotas. Median carbon quotas were 25.7, 22.6, and 5.9 fg C cell^{-1} for populations of the picocyanobacterium *Prochlorococcus*, high-scatter heterotroph, and low-scatter heterotroph, respectively. Carbon-specific rates of primary production as a function of cell size, using the ^{14}C method, and phosphate transport, using ^{33}P radiotracers, resulted in negative power scalings (b) within populations of *Prochlorococcus* and heterotrophs of $b = -1.3$ and $b = -1.1$, respectively. These findings are in contrast to the positive empirical power scaling comprising the broader and larger prokaryote category ($b = 0.7$) and point to within-population variability in cell physiology and metabolism for these important microbial groups.

The empirical scaling of maximal metabolic rates (Y'; mol [mol C]$^{-1}$ h^{-1}) to cell size (M), in the form $Y' = aM^b$, has been carefully studied for nearly two centuries (Sarrus and Rameaux 1839; Robiquet and Tillaye, circa 1839, in Kleiber [1932]). When organisms spanning more than 20 orders of magnitude in body size are compared, a mass-specific scaling exponent (b) of −0.25 accurately predicts metabolic rates. This allometric scaling "law" has been explained by the fractal nature of vascular transport abridging surface area-dependent (proportional to $b = -0.33$) and volume-dependent (proportional to an isometric $b = 0$) rates (West et al. 1997). More recently, other scaling exponents which delineate heterotrophic prokaryotes ($b = 0.72 \pm 0.07$), protists ($b = -0.03 \pm 0.05$), and metazoans ($b = -0.24 \pm 0.08$) have been resolved, citing genome size, endosymbiotic surface area, and vascular transport as constraints (DeLong et al. 2010). Similar superlinear ($b > 0$) mass-specific metabolic rates have been reported within the photoautotrophic prokaryotes (Marañon et al., 2007; Huete-Ortega et al., 2012; García et al. 2015), although the range of estimates is broad ($b = -0.08$ to $b = 0.67$). Allometric scalings are a linchpin of the metabolic theory of ecology (MTE; Brown et al. 2004*a*) and are leveraged for the estimation of maximum intrinsic growth rates and substrate transport rates (Aksnes and Egge 1991; Litchman et al. 2007; Finkel et al. 2010; Edwards et al. 2012), assimilation numbers (Finkel 2001), and elemental stoichiometry (Finkel et al. 2010; Marañon et al. 2013) in "trait-based" ocean ecosystem models (Follows and Dutkiewicz 2011). These parameterizations help to reduce the dimensionality of ecosystem models. An extensive review of allometric relationships for marine phytoplankton is found elsewhere (Marañon 2015).

As Brown et al. of the original MTE paper (Brown et al. 2004*a*) responded to a very active forum on the topic of metabolic rates (Brown et al. 2004*b*), "When body mass differs by only two- or threefold, or temperature varies by only a degree or two, other factors can assume equal or greater importance." At Station ALOHA, the site of the Hawai'i ocean time-series program, that is representative of the North Pacific Subtropical Gyre, microbial particle size distributions within the range 0.2–1.0 μm comprise most of the biomass and photosynthesis (Rii et al. 2016), and sea surface temperatures vary seasonally by only ∼3°C. Accordingly, it should be established if these "other factors," namely metabolic strategies, physiological adaptations, cell cycle stage, and community interactions, are instead the dominant constraints and controls of metabolic rates.

*Correspondence: jrcasey@hawaii.edu

Additional Supporting Information may be found in the online version of this article.

In the surface layer at Station ALOHA, the majority of cells in the <1.0 μm size interval belong to the cyanobacterial genus *Prochlorococcus* and the heterotrophic alphaproteobacterial orders Pelagibacterales (SAR11 clade) and Rhodobacterales (*Roseobacter* clade; Ottesen et al. 2014). We asked if allometric relationships can be used to predict within-population metabolic rates for *Prochlorococcus* and small heterotrophs and whether these relationships are consistent with previous reports of the broader prokaryote size interval. To calculate carbon-specific metabolic rates as a function of body size, we incubated whole microbial communities with specific radio-labeled substrates and then size fractionated cells at 0.05 μm intervals sequentially from 1.00 to 0.10 μm. We also conducted flow cytometric analysis of the sequence of filtrates to infer cellular carbon spectra of the filtered size classes, based on forward-angle light scatter (FSC). Our results indicate a negative power law relating carbon-specific rates of primary production and phosphate uptake to body size within populations, in contrast to a positive power law found between prokaryotic species analyzed over a broader size scale (summarized in Marañon 2015).

Methods

Study site and sample collection

Field experiments were conducted on two expeditions in May 2015 at Station ALOHA (22°45′N, 158°00′W). Water samples were collected from 15 m using a rosette of PVC Bullister bottles mounted on a frame equipped with dual conductivity sensors, dual temperature sensors, pressure sensors, an oxygen sensor, transmissometer, and fluorometer (SBE 911plus, Sea-Bird Electronics). Supporting data from a similar experiment conducted at the same site in September 2013 are included as a supplement to this article (Supporting Information Fig. S1).

Filtration using custom membranes

A series of 47-mm diameter polycarbonate membrane filters spanning the pore size range 0.10–1.00 μm at 0.05 μm intervals were custom fabricated (Sterlitech) to finely size fractionate particles. Five-hundred-milliliter samples were sequentially filtered by gentle vacuum (<70 mbar differential) using a pair of self-contained filter holders and receivers. The collected filtrate was filtered with the next smaller pore size filter using a separate filter holder, and this process was repeated until all fractions were collected. To validate manufacturer-stated pore sizes, filter surfaces (shiny side) were imaged by scanning electron microscopy (SEM; Hitachi S-4800 field emission SEM) fitted with a silicon drift detector (Oxford INCA X-Act energy dispersive spectroscope; Oxford). Images were analyzed by automated detection of pore edges and measuring diameter of at least 20 pores per filter using embedded scale bars (Fiji; Schindelin et al. 2012).

$H^{14}CO_3^-$-assimilation measurements

Rates of inorganic carbon assimilation were measured by the $H^{14}CO_3^-$ tracer method according to standard protocols (Letelier et al. 1996). Five hundred milliliter of seawater was collected in triplicate, inoculated with 100 μCi $H^{14}CO_3^-$ and incubated for 12 h beginning prior to sunrise and terminated after sunset. Deckboard acrylic incubators, shaded to approximately the blue light attenuation at 15 m, were flushed with surface seawater to maintain in situ temperatures. Incubations were terminated by sequential filtration (described above). A 100-μL sample was collected from each incubation and added to a 20-mL scintillation vial containing 0.5 mL β-phenethylamine (Sigma-Aldrich #407267), a CO_2 trap to measure total activity for estimation of specific radioactivity (^{14}C [mol C]$^{-1}$). Filters were placed in 20-mL scintillation vials, acidified with 1-mL 2 mol L^{-1} hydrochloric acid, and allowed to vent for 24 h prior to liquid scintillation counting. The assimilation of ^{14}C-bicarbonate over 12-h incubations approximates a rate between net and gross primary production (Marra 2002; Pei and Laws 2013), referred to herein as ^{14}C-assimilation.

^{33}P-PO_4^{3-} uptake measurements

Phosphate assimilation rates were measured using the radioisotope tracer $^{33}PO_4^{3-}$ (Björkman and Karl 2003). Five hundred milliliter of seawater was collected in triplicate and inoculated with 2.5 μCi L^{-1} carrier-free $^{33}PO_4^{3-}$, which was approximately 0.002% the mass of the ambient soluble reactive phosphorus. Incubations were conducted for 4.5 h as described above, from 0900–1330 h local time. Incubations were terminated by cold chase (0.6 μmol L^{-1} PO_4^{3-} final concentration) prior to sequential filtration and processed similarly to ^{14}C-assimilation filters.

Prochlorococcus culture $H^{14}CO_3^-$ assimilation experiment

Prochlorococcus strain MIT9301 was acclimated for several generations to growth in PRO99 medium (Moore et al. 2007) at 24°C in a 14 h light : 10 h dark cycle reaching a maximum irradiance of 20 μmol quanta m^{-2} s^{-1} blue light. One milliliter aliquots of culture suspension was inoculated with 10 μCi $H^{14}CO_3^-$ for 1 h and terminated by 0.5% paraformaldehyde fixation in the dark at 4°C for 30 min. Fixed samples were diluted to 100 mL 0.2 μm filtered seawater prior to sequential filtration. Filters were processed identically to the above description for natural assemblages. ^{14}C assimilation over this shorter incubation interval more closely approximates gross primary production (Pei and Laws 2013) and therefore cannot be compared directly to 12 h ^{14}C-assimilation field measurements.

Flow cytometry

Samples for flow cytometry were collected from whole seawater samples (prior to filtration) and from all filtrate fractions. One milliliter samples was fixed with paraformaldehyde (0.2 μm syringe filtered; 0.5% final concentration) in the dark at 4°C for 30 min prior to flash freezing in liquid nitrogen and stored at −80°C. Samples were analyzed using a jet-in-air Influx Cell Sorter (BD Biosciences) equipped with a small

particle detector (100X magnification objective in the FSC path) and 200 mW 457 and 488 nm lasers (Coherent) aligned through the same pinhole. Sample pressures were always maintained within 1 psi above the sheath pressure to minimize core width and instability. Analog pulse height signals from 530/20, 580/30, and 692/40 nm bandpass filters were log amplified from photomultiplier tube detectors (Hamamatsu), and data were collected in listmode files using the acquisition software Spigot (BD Biosciences). *Prochlorococcus*, *Synechococcus*, high-scatter (HS) heterotrophs, and low-scatter (LS) heterotrophs were quantified and discriminated based on their autofluorescence and light scattering properties (Casey et al. 2013), as well as their fluorescence of the nucleic acid stain SYBR Green I (Invitrogen; Marie et al. 1997). *Synechococcus* was discriminated from *Prochlorococcus* by its yellow–green fluorescence and larger scattering amplitudes. Polystyrene calibration particles (0.53 μm) impregnated with Nile Red dye (Spherotech) were used for optical and fluidic alignment and as an internal light scatter standard. Approximately 300 μL of unstained and SYBR Green I-stained samples were separately acquired to ensure that a sufficient number of events were recorded. Concentrations were determined by weighing the sample before and after acquisition, taking into account the hold-up volume of the sample tube.

Determination of carbon quotas

A method for quantifying population-specific carbon retained on each filter using sequential filtration was developed. The method converts FSC signals to cellular carbon content using a previously determined calibration curve (Casey et al. 2013) for the InFlux Cell Sorter. FSC data of gated populations and internal standard particles were used to generate normalized FSC histograms. To minimize spurious events at the distribution extremes (which can be important for large, rare particles), distributions were smoothed using a normal kernel function with bin widths scaled to the coefficient of variation of the internal standard particles, and the number of bins set equal to the number of FSC channels. After applying the carbon-FSC calibration, the carbon transformed scale was then used to generate cellular carbon spectra for each filtrate sample using the sequential filtration method. The carbon spectrum of each filtrate was then subtracted from the next largest filtrate spectrum, and the residual spectrum was integrated to calculate total particulate carbon caught on each filter. A repository of the data files, code, and documentation are available as a MATLAB distribution (Supporting Information File S1).

Results

Filtration

SEM imaging was used to quantify the distribution of pore sizes of a representative filter from each batch of each pore size filter used in this study. Filter pore sizes were within ± 2–16% of manufacturer specifications in the 0.10–0.35 μm interval and ± 3–7% in the 0.40–1.00 μm interval. Model I least squares regression of median pore sizes as a function of manufacturer-specified pore sizes was not significantly different from unity (p = 0.81; Fig. 1), and no residuals trend was apparent. Due to the manufacturing process (Karl 2007), pores are arranged in a random spatial distribution, resulting in a density-dependent occurrence of overlap. This artifact could, presumably, allow for the passage of particles larger than the singlet pore diameter. From the total number of pores imaged (n = 21,933), image analysis of electron micrographs revealed a 2–8% frequency of overlap as doublets and <1% as triplets. The sequential filtration technique was, nonetheless, effective at capturing particles larger than the singlet diameter. However, analysis of the FSC distribution of particles caught on each filter revealed a right skewness (1.2 ± 0.6), instead indicating that particles smaller than the singlet diameter were more frequently captured, likely a result of impaction or pore loading.

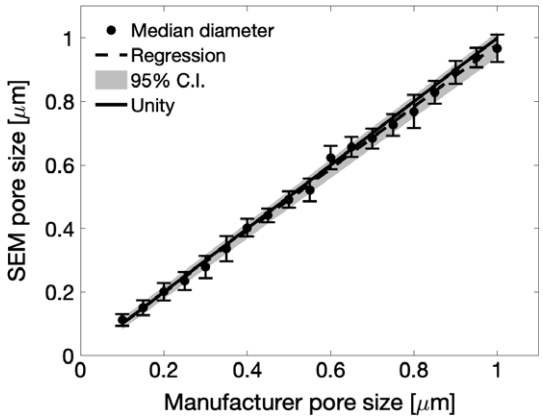

Fig. 1. Comparison of manufacturer-stated pore sizes (median diameter) and SEM-calibrated pore sizes. Data are median values for each filter, and error bars represent one standard deviation of the mean. Also shown are the line of unity (1 : 1; solid line), least squares regression (dashed line), and the 5% and 95% confidence intervals (gray shaded region).

By comparing the sum of differences for each population to their initial concentrations in each sample, we found cell losses within each sample to be <0.01% and <0.1% for *Prochlorococcus* and heterotrophs, respectively. This nearly quantitative recovery indicates no appreciable loss of cells due to lysis or adhesion to the filtration vessel using the sequential filtration technique.

Isolation of picoplankton populations

Prochlorococcus could not be discretely separated by filtration from the total heterotroph population (Fig. 2). Of the total 2.2×10^5 cells mL^{-1}, a majority (80% ± 3%) of *Prochlorococcus* cells could be detected within the 0.30–0.70 μm interval, overlapping both the LS heterotroph interval from 0.25 to 0.45 μm (3.1×10^5 cells mL^{-1}) and the HS heterotroph interval from 0.45 to 0.60 μm (1.1×10^5 cells mL^{-1}). The remaining

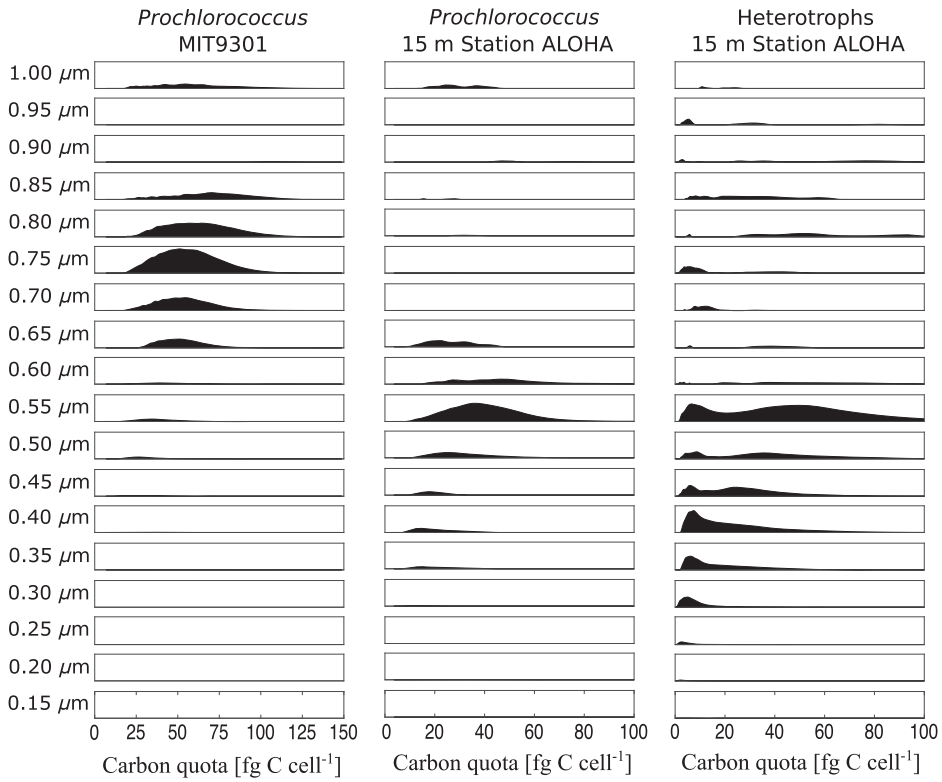

Fig. 2. Histograms of cell carbon quotas retained on each filter, as an average of three replicates. Columns of histograms correspond to *Prochlorococcus* MIT9301 (left column), Station ALOHA *Prochlorococcus* (middle column) and heterotrophs (right column).

20% of *Prochlorococcus* cells and 30% of heterotrophs were captured by larger filter fractions, although the skewness of their respective FSC distributions indicated that they were caught by impaction or pore clogging. The bimodal size spectra of *Prochlorococcus* and heterotrophs are a striking feature, with peaks at 0.55 and 0.40 μm in both populations corresponding to a 1.8–2.6 fold change in cell volume. A more pronounced bimodal size spectrum was observed for *Prochlorococcus* on a separate cruise from the same depth but in September 2013 (Supporting Information Fig. S1). *Synechococcus* was present at low concentrations (479 $\pm$ 77 cells mL^{-1}) and was largely excluded from the sequential filtration interval (70% of cells were larger than 1.00 μm), although a few cells could be detected as low as 0.45 μm.

Size spectrum of picoplankton carbon

Cellular carbon content comprised the range 4–125 fg C cell^{-1} over the 0.10–1.00 μm pore size interval. The resulting carbon density of cells in this range was 240 fg C μm^{-3}, similar to previously reported values which range from 190 to 470 fg C μm^{-3} with a median value of 228 fg C μm^{-3} based on 12 studies (references compiled in Casey et al. [2013]). Cell carbon quotas were log-normally distributed and centered about the median values 25.8, 22.6, and 5.9 fg C cell^{-1} for *Prochlorococcus*, HS heterotrophs, and LS heterotrophs, respectively (Table 1). Exponentially growing *Prochlorococcus* MIT9301 cells, harvested at midday, were markedly larger (0.65–0.80 μm) than the natural population, with an average carbon quota of 57 fg C cell^{-1} (Fig. 3). The sum of carbon retained on filters, as calculated by

Table 1. Summary statistics of cell carbon quotas for natural populations of Prochlorococcus, LS heterotrophs, and HS heterotrophs. Concentrations are reported as 10^5 cells mL^{-1}; all other values are reported as fg C cell^{-1}. All values were computed as the mean $\pm$ standard deviation of three unfiltered seawater samples.

	Prochlorococcus	LS heterotrophs	HS heterotrophs
Concentration (10^5 cells mL^{-1})	2.2 $\pm$ 0.11	4.4 $\pm$ 0.25	1.3 $\pm$ 0.28
Variance (fg C cell^{-1})	234.6 $\pm$ 19.1	16.5 $\pm$ 0.2	193.6 $\pm$ 4.5
Mean (fg C cell^{-1})	27.7 $\pm$ 1.2	6.7 $\pm$ 0.0	26.6 $\pm$ 0.2
Median (fg C cell^{-1})	25.8 $\pm$ 1.1	5.9 $\pm$ 0.0	22.6 $\pm$ 0.5
Standard deviation (fg C cell^{-1})	12.5 $\pm$ 0.6	4.0 $\pm$ 0.0	13.9 $\pm$ 0.2

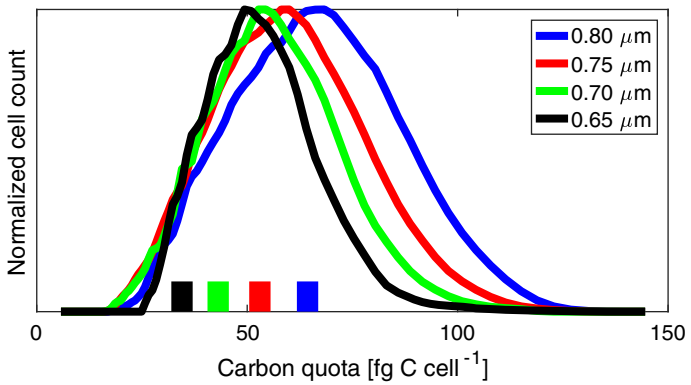

Fig. 3. Cell count-normalized carbon spectrum of *Prochlorococcus* MIT9301 retained on each filter within the interval comprising 91% of the initial population. Vertical bars represent expected carbon quota of cells with equivalent spherical diameter matching the respective pore size. Note the proportion of each distribution with carbon quotas lower than the pore-size–derived carbon quota.

the histogram subtraction method, recovered 107% ± 8% of the initial picoplankton carbon. The discrepancy in summed fractions from the interval total is due to the necessary smoothing function applied to FSC distributions (Supporting Information File S1). *Prochlorococcus* contributed 68% ± 2% (8.9 ± 0.2 μg C L^{-1}) while heterotrophs and *Synechococcus* contributed the remainder (23% ± 1% and 8% ± 0%, respectively) of the total picoplankton carbon (13.2 ± 0.3 μg C L^{-1}). The sum of picoplankton carbon in the measured interval (0.10–1.00 μm) represented 41% ± 2% of particulate carbon as determined by elemental analysis (Hebel and Karl 2001; http://hahana.soest.hawaii.edu/hot/hot-dogs/).

Size spectrum of picoplankton metabolic rates

^{14}C-assimilation varied by roughly an order of magnitude over the *Prochlorococcus* size interval (0.35–0.65 μm), with maxima coinciding with cell number and carbon retained on the 0.55 and 0.40 μm filters (Fig. 4 and Supporting Information Fig. S1). Radioactivity was detectable at low levels in the 0.15–0.35 μm interval (4.95 ± 0.21 nmol L^{-1} h^{-1}; 11% of total ^{14}C-assimilation), where few (<0.1%) or no *Prochlorococcus* cells could be detected. By scaling $^{33}PO_4^{3-}$ assimilation in the same interval to an average of C : P ratios of proteobacterial representatives (77 mol C : 1 mol P; Zimmerman et al. 2014), we can account for 3.17 ± 0.07 nmol L^{-1} h^{-1} of the ^{14}C uptake, likely an indication of heterotrophic uptake of recently fixed photosynthate, chemolithoautotrophy, or anapleurotic carbon fixation. Low levels of ^{14}C-assimilation at larger size intervals (0.70–0.95 μm; 20% of total) were due to low

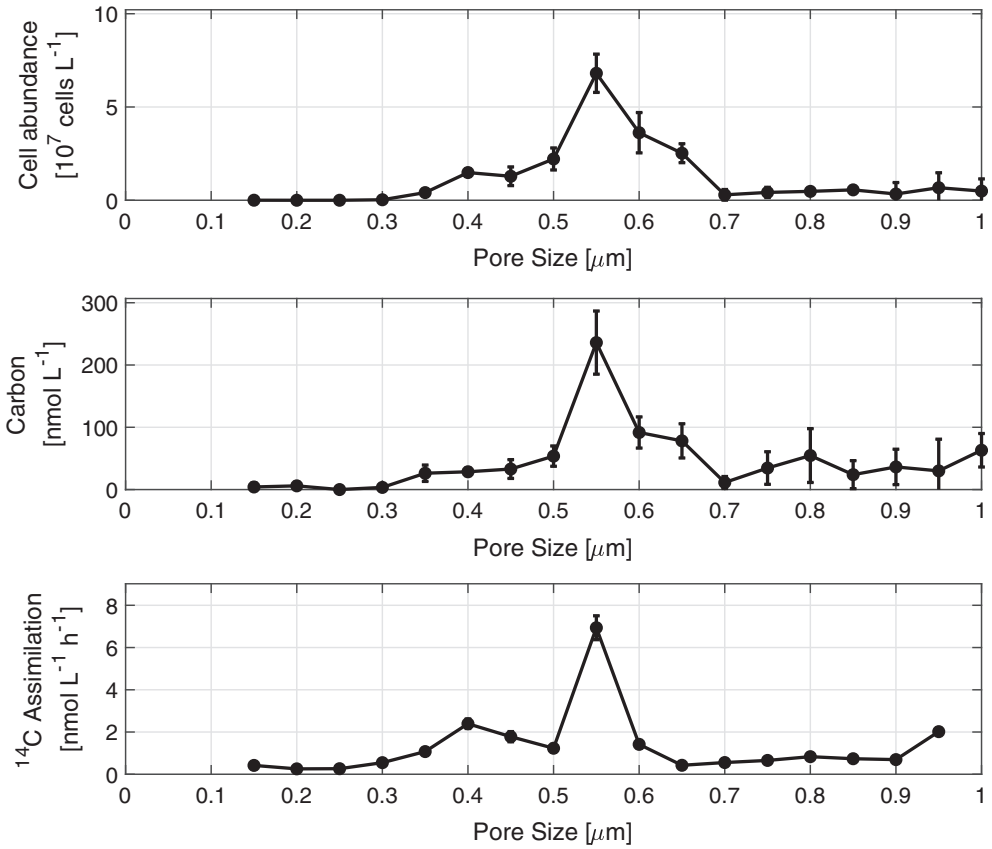

Fig. 4. Size spectrum of the number of *Prochlorococcus* cells (top panel), *Prochlorococcus* carbon (middle panel), and ^{14}C-assimilation (bottom panel). Mean values are shown with error bars representing 1 SD. ^{14}C-assimilation data from the 1-μm filter fraction are excluded.

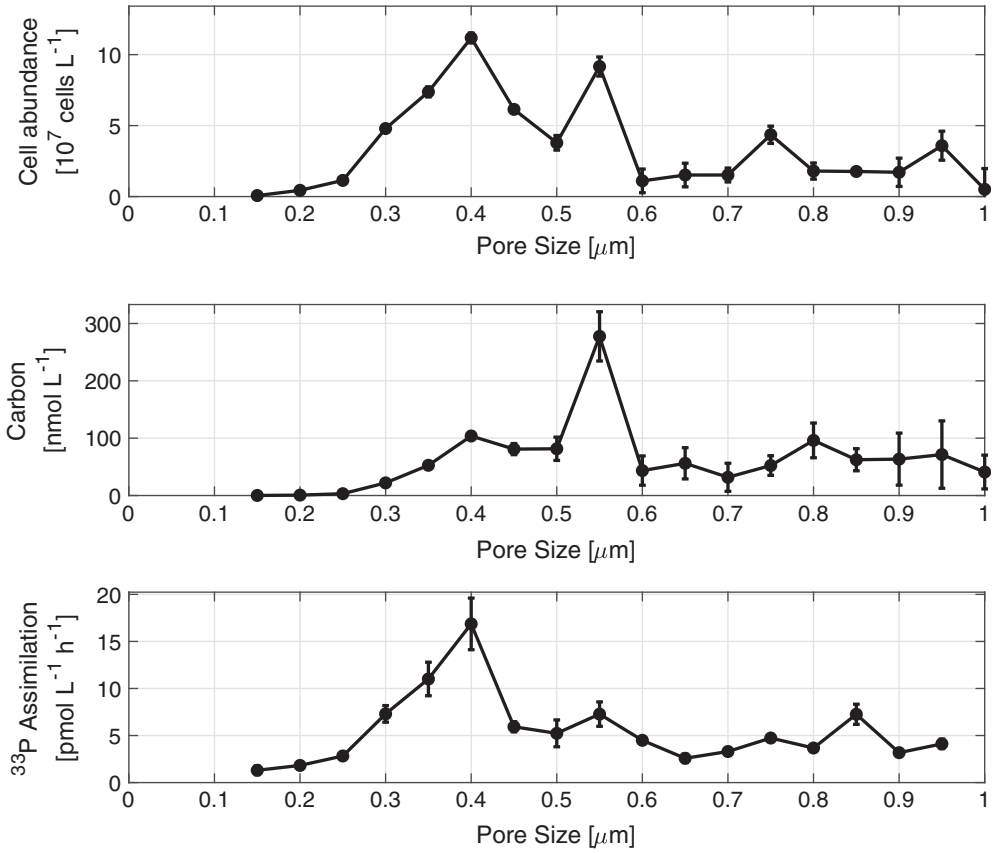

Fig. 5. Size spectrum of the number of *Prochlorococcus* and heterotrophic cells (top panel), *Prochlorococcus* and heterotrophic carbon (middle panel), and $^{33}PO_4^{3-}$ assimilation rates (bottom panel). Mean values are shown with error bars representing 1 SD. $^{33}PO_4^{3-}$ assimilation data from the 1 μm filter fraction are excluded.

concentrations of small *Synechococcus* cells as well as *Prochlorococcus* cells caught on larger pore size filters. ^{14}C-assimilation in the 0.10–1.00 μm interval represented 76% ± 3% of the total community ^{14}C-assimilation (>0.2 μm).

$^{33}PO_4^{3-}$ assimilation also varied by roughly an order of magnitude over the heterotroph and *Prochlorococcus* size interval (0.20–0.65 μm), with maxima coinciding with the LS heterotroph cell number maximum at 0.40 μm and the HS heterotroph and *Prochlorococcus* cell number maximum at 0.55 μm (Fig. 5). LS heterotrophs contributed more than half (51% ± 5%) of the total $^{33}PO_4^{3-}$ assimilation within the <1.00 μm fraction, whereas the *Prochlorococcus* and HS heterotroph populations collectively contributed only 25% ± 3%. $^{33}PO_4^{3-}$ assimilation within the 0.10–1.00 μm interval represented 86% ± 11% of the total community $^{33}PO_4^{3-}$ assimilation (>0.2 μm).

Allometric relationships

Prochlorococcus carbon-specific ^{14}C-assimilation rates (mol C L^{-1} h^{-1} [mol C L^{-1}]$^{-1}$) and picoplankton carbon-specific $^{33}PO_4^{3-}$ assimilation rates (mol P L^{-1} h^{-1} [mol C L^{-1}]$^{-1}$) varied as a power law function of pore size converted to cell volume ($Y' = aM^b$, where C is the cellular carbon content); the calculated exponent b was −1.3 ± 0.4 ($p = 2e^{-7}$) and −1.1 ± 0.4 ($p = 1e^{-5}$), respectively (Fig. 6). We excluded the smallest fractions (<0.35 μm) from the ^{14}C-assimilation calculation as only 2% of the *Prochlorococcus* biomass was captured. By weighting *Prochlorococcus* carbon-specific ^{14}C-assimilation rates to the *Prochlorococcus* carbon size spectrum, the mean population growth rate was 0.58 ± 0.15 d^{-1}, similar to maximal growth rates of high-light adapted ecotypes in culture (0.63 ± 0.06 d^{-1}; Moore et al. 1995). The calculated b for *Prochlorococcus* MIT9301 carbon specific $H^{14}CO_3^-$ assimilation rates was −2.2 ($p = 0.04$; Fig. 6), and the growth rate estimated from the same method was 0.31 d^{-1}.

Discussion

Size fractionation can be an effective tool for probing the variability of physiology and metabolism within natural food web components (Sheldon et al., 1972; Azam and Hodson 1977; Karl 2007) and, at the resolution utilized in this study, within picoplankton populations. Whatever the mechanism, be it flow impaction or pore clogging, it should be recognized that particles smaller than the filter pore size are retained. Depending on the application, this fraction may significantly bias size fractionation results. Accounting for this effect, we

coupled size fractionation of radioisotope incubations to flow cytometric determinations of cellular carbon and observed significant variability in metabolic rates within natural picoplankton populations.

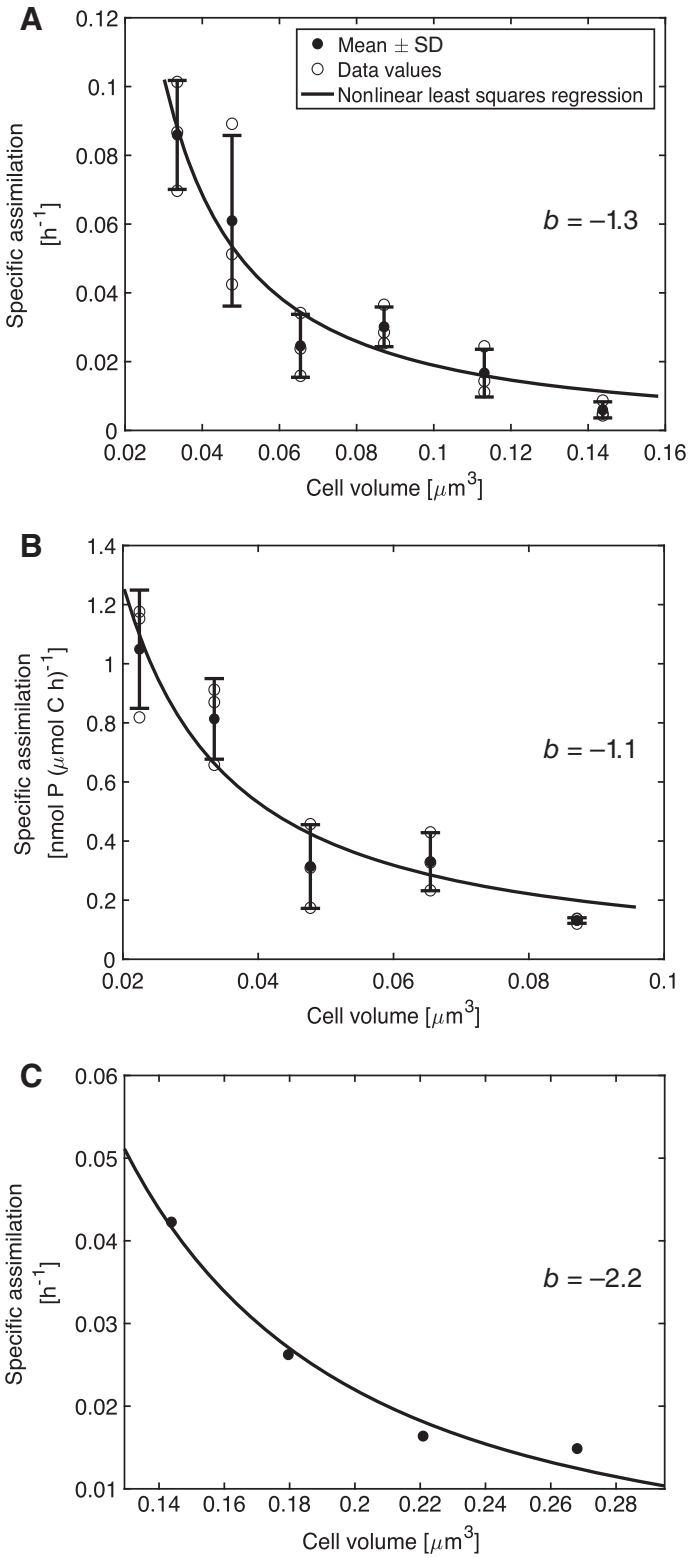

Fig. 6. Allometric relationships. *Prochlorococcus* carbon-specific ^{14}C-assimilation (**A**), *Prochlorococcus* and hetrotrophic carbon-specific $^{33}PO_4^{3-}$ assimilation rates (**B**), and *Prochlorococcus* MIT3901 carbon-specific ^{14}C-assimilation (**C**) plotted as a function of equivalent spherical cell volume (based on pore size). Mean values and replicate data are plotted, and error bars represent 1 SD. Nonlinear least squares fit of the power law regression ($Y = aM^b$) and the corresponding mean b value are also shown.

The sequential filtration method employed in this study quantitatively recovered cells within the 0.10–1.00 μm fraction and resolved cellular carbon content and metabolic rates at 0.05 μm intervals. Using this method, we observed bimodal size distributions in *Prochlorococcus*, which were not apparent in flow cytograms; however, it is likely that traditional flow cytometers do not sufficiently discriminate anisotropic scatterers in this size range to resolve peaks which are separated by only 0.15 μm. For *Prochlorococcus*, this distribution may either be due to the cell cycle stage distribution (this interval corresponds to a 1.8–2.6 fold change in cell volume) or due to physiological differences between strains. The latter has been observed at Station ALOHA, especially near the deep chlorophyll maximum depth (Campbell and Vaulot 1993) or following a deepening of the mixed layer, which transiently mixes the low-light adapted and high-light adapted *Prochlorococcus* populations (Thompson et al. 2018); however, these bimodal distributions are prominent in flow cytograms rather than the subtle differences we observed.

The relationships between carbon-specific primary productivity or phosphate assimilation rates and cell size differed in our study from those predicted by the broader prokaryote allometric relationship (e.g., García et al., 2015). In natural *Prochorococcus* populations, heterotrophic populations, and a *Prochlorococcus* isolate MIT9301, the exponents were all negative ($b = -1.3$, $b = -1.1$, and $b = -2.2$, respectively) rather than positive ($b = 0.72$; DeLong et al. 2010), suggesting that the within-population allometric relationship is independent of the allometric relationships observed between populations. In both natural populations and a laboratory isolate, the observed scaling factor indicates that the smallest cells are disproportionately active. In the case of *Prochlorococcus*, which is phase locked to the solar cycle for initiation of cell division (Vaulot et al. 1995; Liu et al. 1997), it is possible that larger cells are arrested in cell cycle stage. Remnants of the previous day's cycle, perhaps these cells, require very little additional resources to satisfy the remaining carbon and energy quota and are simply awaiting the signaling cascade to initiate genome replication and division. We offer the hypothesis that metabolic rates slow as cells approach the threshold for division. Although such a synchronicity has not yet been reported for heterotrophic picoplankton, diel rhythms in proteobacterial gene expression are widespread (Ottesen et al. 2014; Aylward et al. 2015) and, like

the photoautotrophs they depend on, replication may be entrained to the light cycle.

The empirical allometric power law is a useful approximation of ecosystem function when the size distribution of organisms spans several orders of magnitude. However, the universal $b = -0.25$ is apparent only when organisms spanning many orders of magnitude in body size are grouped and has been challenged by closer inspection of b between microbial taxa (reviewed in Marañon [2015]). At the smallest scales (<1 μm), the size dependence of microbial metabolism had not until recently (García et al. 2015) been investigated in natural marine bacterioplankton populations and thus the lower extent of the size range which applies to the prokaryotes. Our results do not refute previously reported allometric relationships within the prokaryotes; however, we demonstrate that within the size spectrum of the smallest prokaryotes exists a structuring of metabolic rates that do not scale with broader cell size comparisons. The genetic, regulatory, metabolic, and physiological mechanisms that underlie our observations, and which provide the basis for our interpretation that *Prochlorococcus* metabolism slows as cells approach division, should be further investigated.

References

Aksnes, D. L., and J. K. Egge. 1991. A theoretical model for nutrient uptake in phytoplankton. Mar. Ecol. Prog. Ser. **70**: 65–72. doi:10.3354/meps070065

Aylward, F. O., J. M. Eppley, J. M. Smith, F. P. Chavez, C. A. Scholin, and E. F. DeLong. 2015. Microbial community transcriptional networks are conserved in three domains at ocean basin scales. Proc. Natl. Acad. Sci. USA **112**: 5443–5448. doi:10.1073/pnas.1502883112

Azam, F., and R. E. Hodson. 1977. Size distribution and activity of marine heterotrophs. Limnol. Oceanogr. **22**: 492–501. doi:10.4319/lo.1977.22.3.0492

Björkman, K. M., and D. M. Karl. 2003. Bioavailability of dissolved organic phosphorus in the euphotic zone at station ALOHA, North Pacific Subtropical Gyre. Limnol. Oceanogr. **48**: 1049–1057. doi:10.4319/lo.2003.48.3.1049

Brown, J. H., J. F. Gillooly, A. P. Allen, V. M. Savage, and G. B. West. 2004*a*. Toward a metabolic theory of ecology. Ecology **85**: 1771–1789. doi:10.1890/03-9000

Brown, J. H., J. F. Gillooly, A. P. Allen, V. M. Savage, and G. B. West. 2004*b*. Response to forum commentary on "toward a metabolic theory of ecology.". Ecology **85**: 1818–1821. doi:10.1890/03-0800

Campbell, L., and D. Vaulot. 1993. Photosynthetic picoplankton community structure in the subtropical North Pacific Ocean near Hawaii (station ALOHA). Deep-Sea Res. Part I: Oceanogr. Res. Pap. **40**: 2043–2060. doi:10.1016/0967-0637(93)90044-4

Casey, J., J. P. Aucan, S. R. Goldberg, and M. W. Lomas. 2013. Changes in partitioning of carbon amongst photosynthetic pico- and nano-plankton groups in the Sargasso Sea in response to changes in the North Atlantic oscillation. Deep-Sea Res. Part II: Top. Stud. Oceanogr. **93**: 58–70. doi:10.1016/j.dsr2.2013.02.002

DeLong, J. P., J. G. Okie, M. E. Moses, R. M. Sibly, and J. H. Brown. 2010. Shifts in metabolic scaling, production, and efficiency across major evolutionary transitions of life. Proc. Natl. Acad. Sci. USA **107**: 12941–12945. doi:10.1073/pnas.1007783107

Edwards, K. F., M. K. Thomas, A. Klausmeier, and E. Litchman. 2012. Allometric scaling and taxonomic variation in nutrient utilization traits and maximum growth rate of phytoplankton. Limnol. Oceanogr. **57**: 554–566. doi:10.4319/lo.2012.57.2.0554

Finkel, Z. V. 2001. Light absorption and size scaling of light-limited metabolism in marine diatoms. Limnol. Oceanogr. **46**: 86–94. doi:10.4319/lo.2001.46.1.0086

Finkel, Z. V., J. Beardall, K. J. Flynn, A. Quigg, T. A. V. Rees, and J. A. Raven. 2010. Phytoplankton in a changing world: Cell size and elemental stoichiometry. J. Plankton Res. **32**: 119–137. doi:10.1093/plankt/fbp098

Follows, M. J., and S. Dutkiewicz. 2011. Modeling diverse communities of marine microbes. Ann. Rev. Mar. Sci. **3**: 427–451. doi:10.1146/annurev-marine-120709-142848

García, F. C., E. E. García-Martín, F. G. Taboada, S. Sal, P. Serret, and Á. López-Urrutia. 2015. The allometry of the smallest: Superlinear scaling of microbial metabolic rates in the Atlantic Ocean. ISME J. **10**: 1029–1036. doi:10.1038/ismej.2015.203

Hebel, D. V., and D. M. Karl. 2001. Seasonal, interannual and decadal variations in particulate matter concentrations and composition in the North Atlantic subtropical gyre. Deep-Sea Res. Part II: Top. Stud. Oceanogr. **48**: 1669–1695. doi:10.1016/S0967-0645(00)00155-7

Huete-Ortega, M., P. Cermeño, A. Calvo-Díaz, and E. Marañon. 2015. Isometric size-scaling of metabolic rate and the size abundance distribution of phytoplankton. Proceedings of the Royal Society B **279**: 1815–1823. doi:10.1098/rspb.2011.2257

Karl, D. M. 2007. Plastics-irradiated-etched: The Nucleopore® filter turns 45 years old. Limnol. Oceanogr.: Bull. **16**: 49–54. doi:10.1002/lob.200716349

Kleiber, M. 1932. Body size and metabolism. J. Agric. Sci. **6**: 315–353. doi:10.3733/hilg.v06n11p315

Letelier, R. M., J. E. Dore, C. D. Winn, and D. M. Karl. 1996. Seasonal and interannual variations in photosynthetic carbon assimilation at station ALOHA. Deep-Sea Res. II Top. Stud. Oceanogr. **43**: 467–490. doi:10.1016/0967-0645(96)00006-9

Litchman, E., C. A. Klausmeier, O. M. Schofield, and P. G. Falkowski. 2007. The role of functional traits and trade-offs in structuring phytoplankton communities: Scaling from cellular to ecosystem level. Ecology **10**: 1170–1181. doi:10.1111/j.1461-0248.2007.01117.x

Liu, H., H. A. Nolla, and L. Campbell. 1997. *Prochlorococcus* growth rate and contribution to primary production in the

equatorial and subtropical North Pacific Ocean. Aquat. Microb. Ecol. **12**: 39–47. doi:10.3354/ame012039

Marañon, E., P. Cermeño, J. Rodríguez, M. V. Zubkov, and R. P. Harris. 2007. Scaling of phytoplankton photosynthesis and cell size in the ocean. Limnology and Oceanography **52**: 2190–2198. doi:10.4319/lo.2007.52.5.2190

Marañon, E. 2015. Cell size as a key determinant of phytoplankton metabolism and community structure. Ann. Rev. Mar. Sci. **7**: 241–264. doi:10.1146/annurev-marine-010814-15955

Marañon, E., P. Cermeño, D. C. López Sandoval, T. Rodríguez Ramos, C. Sobrino, M. Huete Ortega, J. M. Blanco, and J. Rodríguez. 2013. Unimodal size scaling of phytoplankton growth and the size dependence of nutrient uptake and use. Ecol. Lett. **16**: 371–379. doi:10.1111/ele.12052

Marie, D., F. Partensky, S. Jaquet, and D. Vaulot. 1997. Enumeration and cell cycle analysis of natural population of marine picoplankton by flow cytometry using the nucleic acid stain SYBR green I. Appl. Environ. Microbiol. **63**: 186–193.

Marra, J. 2002. Approaches to the measurement of plankton production, p. 78–108. *In* P. J. l B. Williams, D. N. Thomas, and C. S. Reynolds [eds.], Phytoplankton productivity: Carbon assimilation in marine and freshwater ecosystems. Blackwells. ISBN: 978-0-632-05711-5

Moore, L. R., R. Goericke, and S. W. Chisholm. 1995. Comparative physiology of *Synechococcus* and *Prochlorococcus*: Influence of light and temperature on growth, pigments, fluorescence and absorptive properties. Mar. Ecol. Prog. Ser. **116**: 259–275. doi:10.3354/meps116259

Moore, L. R., and others. 2007. Culturing the marine cyanobacterium *Prochlorococcus*. Limnol. Oceanogr.: Methods **5**: 353–362. doi:10.4319/lom.2007.5.353

Ottesen, E. A., C. R. Young, S. M. Gifford, J. M. Eppley, R. Marin, S. C. Schuster, C. A. Scholin, and E. F. DeLong. 2014. Multispecies diel transcriptional oscillations in open ocean heterotrophic bacterial assemblages. Science **345**: 207–212. doi:10.1126/science.1252476

Pei, S., and E. A. Laws. 2013. Does the ^{14}C method estimate net photosynthesis? Implications from batch and continuous culture studies of marine phytoplankton. Deep-Sea Res. Part I **82**: 1–9. doi:10.1016/j.dsr.2013.07.011

Rii, Y. M., D. M. Karl, and M. J. Church. 2016. Temporal and vertical variability in picophytoplankton primary productivity in the North Pacific Subtropical Gyre. Mar. Ecol. Prog. Ser. **562**: 1–18. doi:10.3354/meps11954

Sarrus, P., and J.-F. Rameaux. 1839. Application des sciences accessoires et principalement des mathématiques àla physiologie générale. Bull. Acad. R. Med. **3**: 1094–1100.

Schindelin, J. E., and others. 2012. Fiji: An open-source platform for biological-image analysis. Nat. Methods **9**: 676–682. doi:10.1038/nmeth.2019

Sheldon, R. W., A. Prakash, and W. H. Sutcliffe. 1972. The size distribution of particles in the ocean. Limnol. Oceanogr. **17**: 327–340. doi:10.4319/lo.1972.17.3.0327

Thompson, A. W., G. van den Engh, N. A. Ahlgren, K. Kouba, S. Ward, S. T. Wilson, and D. M. Karl. 2018. Dynamics of *Prochlorococcus* diversity and photoacclimation during short-term shifts in water column stratification at station ALOHA. Front. Mar. Sci. **5**: 488. doi:10.3389/fmars.2018.00488

Vaulot, D., D. Marie, R. J. Olson, and S. W. Chisholm. 1995. Growth of *Prochlorococcus*, a photosynthetic prokaryote, in the equatorial Pacific Ocean. Science **268**: 1480–1482. doi:10.1126/science.268.5216.1480

West, G. B., J. H. Brown, and B. J. Enquist. 1997. A general model for the origin of allometric scaling laws in biology. Science **276**: 122–126. doi:10.1126/science.276.5309.122

Zimmerman, A. E., S. D. Allison, and A. C. Martiny. 2014. Phylogenetic constraints on elemental stoichiometry and resource allocation in heterotrophic marine bacteria. Environ. Microbiol. **16**: 1398–1410. doi:10.1111/1462-2920.12329

Acknowledgments

We are grateful to T. M. Carvalho and the Biological Electron Microscope Facility at the University of Hawai'i, Manōa for providing SEM images and to the captain and crew of the R/V *Kilo Moana* for their essential support. This work was supported in part by the National Science Foundation (Center for Microbial Oceanography: Research and Education grant DBI 0424599 to D.M.K.; Graduate Research Fellowship to J.R.C.), by the Gordon and Betty Moore Foundation (grant 3794 to D.M.K.), and by the Simons Foundation (Simons Collaboration on Ocean Processes and Ecology award ID 329108 to D.M.K. and Simons Collaboration on Computation Biogeochemical Modeling of Marine Ecosystems/CBIOMES grant 549894 to J.R.C).

Conflict of Interest

None declared

Submitted 13 August 2018
Revised 03 January 2019
Accepted 01 February 2019

Associate editor: Thomas Anderson